SCIENCE CHINA Materials ARTICLES

mater.scichina.com link.springer.com

Published online 25 January 2021 | https://doi.org/10.1007/s40843-020-1552-7
Sci China Mater 2021, 64(6): 1343–1354

Constructing high gravimetric and volumetric capacity sulfur cathode with $LiCoO_2$ nanofibers as carbon-free sulfur host for lithium-sulfur battery

Ya-Tao Liu[†], Lu Wang[†], Sheng Liu, Guo-Ran Li and Xue-Ping Gao[*]

ABSTRACT **Although the gravimetric energy density of lithium-sulfur battery is very encouraging, the volumetric energy density still remains a challenge for the practical application. To achieve the high volumetric energy density of battery, much attention should be paid to the sulfur cathode. Herein, we introduce heavy lithium cobalt oxide ($LiCoO_2$) nanofibers as sulfur host to enhance the volumetric capacity of cathode, maintaining the high gravimetric capacity simutaneously. With the high tap density of 2.26 g cm^{-3}, $LiCoO_2$ nanofibers can be used to fabricate a really compact sulfur cathode, with a density and porosity of 0.85 g cm^{-3} and 61.2%, respectively. More importantly, $LiCoO_2$ nanofibers could act as an efficient electrocatalyst for enhancing the redox kinetics of sulfur species, ensuring the cathode electroactivity and alleviating the shuttle effect of polysulfides. Therefore, a balance between compact structure and high electrochemical activity is obtained for the sulfur cathode. At the sulfur loading of 5.1 mg cm^{-2}, high volumetric and gravimetric capacities of 724 mA h $cm^{-3}_{cathode}$ and 848 mA h $g^{-1}_{cathode}$ could be achieved based on the cathode volume and weight, respectively. Moreover, with this efficient S/$LiCoO_2$ cathode, the lithium corrosion by polysulfides is supressed, leading to a more stable lithium anode.**

Keywords: lithium-sulfur battery, sulfur cathode, volumetric energy density, lithium cobalt oxide, catalytic activity

INTRODUCTION

Lithium-sulfur (Li-S) battery is considered as the most promising energy storage technology beyond lithium-ion batteries (LIBs), due to the high energy densities of 2600 W h kg^{-1} or 2800 W h L^{-1} based on mass or volume consideration, respectively [1–3]. With the overall reaction of 2Li + S = Li_2S, some fundamental issues exist in Li-S chemistry, including the insulation of sulfur/Li_2S, the volume variation of the cathode during cycling, the shuttle of soluble intermediate lithium polysulfides (LiPS) in ether-based electrolyte, and dendrites/cracks on lithium anode [4–5]. In the past decade, great efforts have been made to tackle these issues, such as employing sophisticated cathode structure [6–8], heteratom-doped carbon [9–11], polar compounds [12–16], interlayers [17–18], functional separators [19–20], novel binders [21–22], and stabilized anode [23–26]. As a result, the battery performance has improved to a large extent. For instance, the gravimetric energy density (W_G) of pouch Li-S cell has reached 300–600 W h kg^{-1} in recent years, and researchers are ready to put Li-S battery into markets for specific applications, such as unmanned aerial vehicle, e-buses, trucks and marine devices [27–29]. Despite the attractive W_G, however, the volumetric energy density (W_V) is limited within ca. 325 W h L^{-1} for Li-S battery, far behind LIBs (~700 W h L^{-1}) [30–31]. The low W_V is a critical challenge for the practical application of Li-S battery with a confined space, and might undermine its possible market interests in electric vehicles [31]. Therefore, W_V should be paid more attention to in order to fully achieve the potential of Li-S battery [31–33].

Intrinsically, the low W_V of Li-S battery stems from the low density of sulfur (2.07 g cm^{-3}), in comparison with the intercalation compounds as cathode in LIBs. The light-weight sulfur makes it hard to construct high density sulfur cathode (S-cathode), and this situation is further aggravated when a large amount of carbon nanomaterials with a low density are used as sulfur host [34]. Recently, some attempts have been made to increase the S-cathode density, including increasing the sulfur content [35], employing compact carbon [36–38], and

Institute of New Energy Material Chemistry, School of Materials Science and Engineering, Nankai University, Tianjin 300350, China
[†] These authors contributed equally to this work.
[*] Corresponding author (email: xpgao@nankai.edu.cn)

fabricating dense cathode structure [39–42]. The volumetric capacity is enhanced in these publications, but there is still room for further improvement as these studies are still limited by carbon nanomaterials as host. Generally, calendering technology could tune the cathode porosity and increase the density, leading to an improved volumetric capacity [43–44]. However, the resultant dense structure by pressure often slows down the sulfur redox due to the poor electrolyte wetting and Li_2S_2/Li_2S deposition, which are harmful to the gravimetric capacity [32,45–46].

To face this challenge, it is necessary to develop alternative approaches with carbon-free and heavy host. Intrinsically, pure sulfur could provide a high volumetric capacity (theoretical 3444 mA h cm^{-3}). However, it appears impossible to use sulfur alone as cathode because of its insulation nature. Usually, the S-cathode consists of sulfur, host materials, binder and conductive agent, where sulfur is distributed on host materials to form the sulfur-based composite (S-composite). The host materials could be classified into two categories in terms of density: heavy one with higher density, and light one with lower density as compared with sulfur. By introducing heavy metal oxides or sulfides, the high volumetric capacity could be obtained for the compact S-composites [32,47–53]. Most recently, Mo_6S_8 and $Ti_3C_2T_x$ are reported to act as heavy sulfur host to build high-density S-cathode [54–55]. Although high volumetric capacity is presented, the gravimetric capacity still needs to be enhanced because of the low sulfur content in cathode (<60 wt%).

In this study, for the first time, we used heavy lithium cobalt oxide ($LiCoO_2$) nanofibers as sulfur host to enhance the volumetric capacity and simultaneously keep the high gravimetric capacity. $LiCoO_2$ nanofibers have several unique advantages. First, $LiCoO_2$, as a typical LIB cathode material, has a high electronic conductivity (~10^{-3} S cm^{-1}) [56]. The conductive networks fabricated by the $LiCoO_2$ nanofibers would facilitate the electron transfer, and a high sulfur fraction of 58–71 wt% in cathode can be easily achieved. Second, $LiCoO_2$ is demonstrated to be an efficient electrocatalyst for enhancing the oxygen evolution reaction (OER) and oxygen reduction reaction (ORR) [57–58]. As sulfur and oxygen belongs to the same group in periodic table, $LiCoO_2$ is expected to potentially accelerate the sulfur redox kinetics, which alleviates the shuttle issue by decreasing the LiPS accumulation at the cathode side and therefore improves the cycle life of Li-S battery. Third, $LiCoO_2$ possesses a true density and tap density up to 5.1 and 2.4–2.9 g cm^{-3}, respectively [59–60], much higher than those of carbon nanomaterials (2.2 and ~0.3 g cm^{-3}, respectively) [32]. The high density feature of $LiCoO_2$ is favorable to construct a compact S-cathode. Therefore, both the high gravimetric and volumetric capacities could be achieved for the compact cathode after using $LiCoO_2$ nanofibers as sulfur host, which is essential for the practical application of Li-S battery.

EXPERIMENTAL SECTION

Materials

Sublimed sulfur (99.5%) and 1,3-dioxolane (99.8%) were purchased from Sigma-Aldrich. $LiNO_3$ and 1,2-dimethoxyethane (DME) were purchased from Alfa Aesar. *N*,*N*-dimethylformamide (DMF, 99.9%), lithium bis(trifluoromethanesulfonyl)imide (99%) and polyacrylonitrile (molecular weight of 150,000) were purchased from J&K. Lithium acetate (99%) and cobalt acetate tetrahydrate (99.5%) were purchased from Macklin. Carboxymethyl cellulose sodium and styrene butadiene rubber were purchased from Shenzhen Kejing Star Technology company. All chemicals were used without further purification.

Preparation of $LiCoO_2$ nanofibers and S/$LiCoO_2$ composite

$LiCoO_2$ nanofibers were prepared by an electrospinning-calcination method. First, precursor fibers were prepared by electrospinning the solution of DMF, polyacrylonitrile, lithium acetate, and cobalt acetate tetrahydrate, and then the precursor fibers were calcined at 650°C for 3 h in air at a heating rate of 1°C min^{-1}. The distance and voltage between the nozzle and collector were 12 cm and 15 kV, respectively, with a flow rate of 20 μL min^{-1}. Carbon nanotubes (CNT) were bought from Nanjing XFNANO Materials Tech. Co., Ltd. The sulfur-based composites were obtained by the melt-diffusion method. Typically, sublimed sulfur and $LiCoO_2$ nanofibers or CNT were first ground using an agate mortar, and then the well mixed powders were sealed in Ar-filled Teflon vessel and heated at 155°C for 12 h with a heating rate of 3°C min^{-1}.

Characterization

The morphology and structures of $LiCoO_2$ nanofibers were characterized by scanning electron microscope (SEM, JEOL, JSM-7800F) and transmission electron microscope (TEM, JEOL, JEM-2800). The crystalline structure was investigated by X-ray diffraction (XRD, Rigaku mini FlexII). The chemical state was analyzed by X-ray photoelectron spectroscopy (XPS, Thermo Scientific ESCALAB 250Xi). The sulfur content was measured by

thermogravimetry (TG, METTLER TOLEDO, TGA/DSC1) and the specific surface area and pore distribution were tested by using Brunauer-Emmett-Teller method (BET, JW-BK112 system). The polysulfides in solution was examined by UV-vis measurement (Varian Cary 100 Conc).

Electrochemical measurement

The S-cathode was prepared by casting the aqueous slurry of S-composite, conductive agent, and binder on current collector. The sulfur loading was controlled by adjusting the slurry thickness. The conductive agent was graphene, and the binder consisted of carboxymethyl cellulose sodium (60 wt%) and styrene butadiene rubber (40 wt%). The cathode was dried first in air circulation oven and then vacuum oven at 60°C for solvent removal. The cathode was cut into a round disk with the diameter of 12 mm. The metal lithium foil was bought from China Energy Lithium Co., LTD., and the lithium anode had the diameter and thickness of 16 and 0.6 mm, respectively. CR2032 coin cells were assembled using S-cathode, lithium anode, Celgard 2300 separator, and the electrolyte composed of lithium bis(trifluoromethanesulfonyl)imide (1 mol L^{-1}) and $LiNO_3$ additive (2 wt%) in 1,3-dioxolane (DOL) and DME (1:1, *v*/*v*). The electrolyte/sulfur (E/S) ratio was 5–10 μL mg^{-1}. The galvanostatic discharge-charge processes were tested on LAND-CT2001A instruments (1 C = 1672 mA g^{-1}) and the cyclic voltammetry (CV) measurement was performed on a CHI 600e electrochemical station. For CV measurement, Al foil was used as current collector, and for battery cycling, carbon paper (TORAY TGP-H-060) was used as current collector.

Electrode porosity (ε)

ε was determined using the following equation [61]:

$$\varepsilon = 1 - \frac{m_{\text{areal}}\left(\frac{w_{\text{sulfur}}}{\rho_{\text{sulfur}}}+\frac{w_{\text{host}}}{\rho_{\text{host}}}+\frac{w_{\text{conductive}}}{\rho_{\text{conductive}}}+\frac{w_{\text{CMC}}}{\rho_{\text{CMC}}}+\frac{w_{\text{SBR}}}{\rho_{\text{SBR}}}\right)}{L}, \quad (1)$$

where m_{areal} (g cm^{-2}) is the mass loading of the electrode except current collector, L (cm) is the electrode thickness, and w (%) and ρ (g cm^{-3}) are the mass fraction and real density of each component, respectively.

Exchange current density (j_0)

The electrochemical surface area (ECSA) was determined by the CV method in a three-electrode electrochemical cell, with $LiCoO_2$ or CNT as the working electrode, platinum as the counter electrode, Ag/AgCl as the reference electrode and 5 mmol L^{-1} $K_3[Fe(CN)_6]$ in 1 mol L^{-1} KCl solution as the electrolyte. The CV scans were tested from 10 to 100 mV s^{-1} in the electrochemical window of 0–0.6 V (*vs.* Ag/AgCl). The diffusion coefficient of 5 mmol L^{-1} $K_3[Fe(CN)_6]$ in 1 mol L^{-1} KCl is 0.76×10^{-5} cm^2 s^{-1}, and the ECSA could be calculated based on the linear relationship between the peak current and square root of scan rate. For j_0, linear sweep voltammetry (LSV) was tested by using $LiCoO_2$ or CNT as the working electrode, lithium foil as the counter and reference electrode in a three-electrode electrochemical cell, with 30 mmol L^{-1} Li_2S_4 and 1 mol L^{-1} LiTFSI in DME as the electrolyte. j_0 was derived from the Tafel plot of current density-voltage (*J*-*V*) curves.

RESULTS AND DISCUSSION

To obtain $LiCoO_2$ nanofibers, composite fibers of polyacrylonitrile (PAN), lithium acetate, and cobalt acetate tetrahydrate were first prepared by electrospinning, and then the composite fibers were calcinated at 650°C for 3 h in air atmosphere. During calcination, PAN was decomposed and the acetates were reacted with oxygen to form crystalline $LiCoO_2$. By optimizing the ratio of PAN and acetates, $LiCoO_2$ could retain an apparent nanofiber morphology with a length of tens of micrometers (Fig. 1a). The nanofibers were built up with small irregular nanocrystals with clear open tips (Fig. 1b), and the hollow nanofibers have an outer diameter of about 600 nm. The formation of the scraggly surface and hollow channel is due to the $LiCoO_2$ shrinkage and gas expansion from PAN decomposition. Specifically, the diameter of the channel and the outer thickness of the single nanofiber are around 470 and 65 nm, respectively. The hollow nanofibers could provide enough space for sulfur accommodation and form conductive networks for electron transportation. High-resolution TEM (HRTEM) image displays the clear lattice fringes of 0.47 and 0.2 nm, corresponding to the exposed (003) and (104) planes (Fig. 1d). The selected area electron diffraction (SAED) pattern shows the diffraction rings of (003), (101), (104) and (110) planes (Fig. 1e). Fig. 1f shows the XRD pattern of the layered $LiCoO_2$ (JCPDS 50-0653), in good agreement with the results of HRTEM and SAED.

Characterization of $LiCoO_2$ nanofibers

The chemical state of $LiCoO_2$ surface was characterized by XPS. Fig. 2a shows the Co 2p core level, including the Co $2p_{1/2}$, Co $2p_{3/2}$ and satellite peaks of Co(II). The binding energies at 779.97 and 780.60 eV are attributed to the Co(III) and Co(II), respectively. In the O 1s core level,

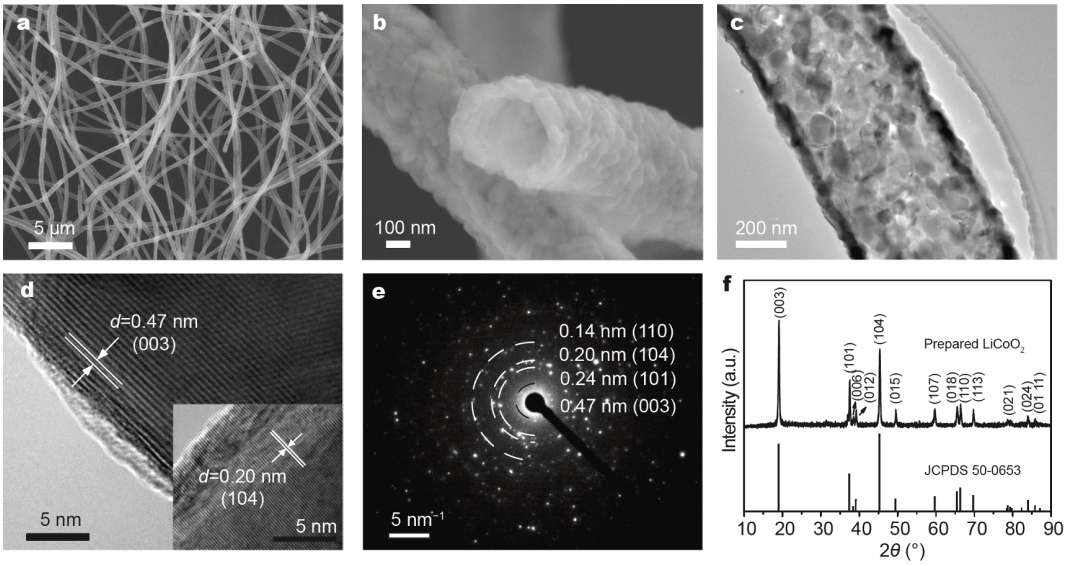

Figure 1 Characterization of $LiCoO_2$ nanofibers. (a, b) SEM images. (c) TEM image. (d) HRTEM image. (e) Selected area electron diffraction (SAED) pattern. (f) XRD pattern.

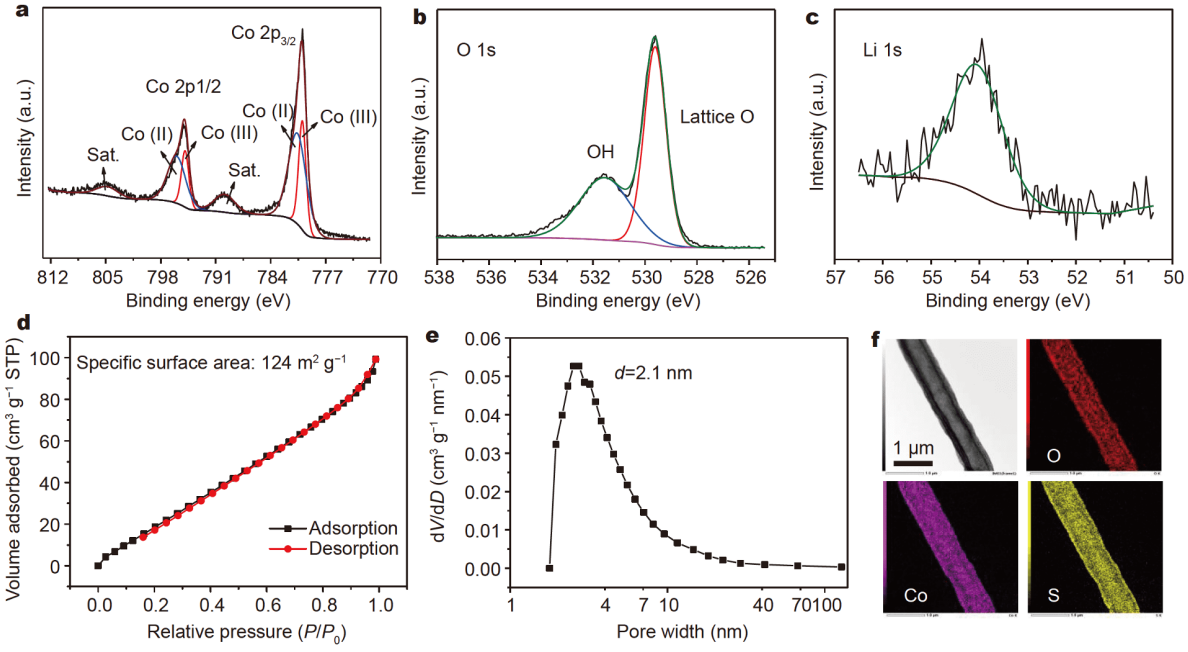

Figure 2 Characterization of $LiCoO_2$ nanofibers and S/$LiCoO_2$ composite. XPS of $LiCoO_2$: (a) Co 2p, (b) O 1s and (c) Li 1s. (d) Nitrogen sorption isotherms of $LiCoO_2$ nanofibers. (e) Pore width distribution of $LiCoO_2$ nanofibers. (f) EDS of S/$LiCoO_2$ composite.

the peak at 529.60 eV is assigned to the lattice oxygen, while the peak at 531.54 eV is attributed to the defective sites within the oxide, adsorbed oxygen or hydroxide species (Fig. 2b) [62]. The spectral area at binding energy range of 52–56 eV is the contribution of Li 1s (Fig. 2c). The nitrogen sorption test shows that $LiCoO_2$ nanofibers have a BET surface area of 124 $m^2 g^{-1}$, with dominant mesopores of ca. 2.1 nm (Fig. 2d, e). The S/$LiCoO_2$ composite was prepared by the typical melt-diffusion method, and energy dispersive spectra (EDS) show that sulfur is successfully infiltrated into the hollow channel of $LiCoO_2$ nanofibers, with oxygen and cobalt uniformly

distributing along the nanofiber (Fig. 2f).

Electrochemical performance of S/$LiCoO_2$ cathode

The cathode is composed of the S/$LiCoO_2$ composite, graphene as a conductive agent, and carboxymethyl cellulose sodium (CMC) and styrene butadiene rubber (SBR) as the binder. Sulfur fraction (w) in the cathode is a highly important parameter for calculating the sulfur capacity (Q_s) and cathode capacity (Q_c) by the relation of $Q_c = Q_s \times w$. Therefore, four cathodes with different sulfur contents (58, 64, 67 and 71 wt%) were prepared in order to find out the optimized sulfur fraction (Fig. S1). The discharge capacity and capacity retention are shown in Fig. 3. Clearly, the cathode with 64 wt% sulfur shows the highest cathode capacity in the initial cycle at 0.25 mA cm^{-2} and 15th cycle at 0.50 mA cm^{-2}. The cathode consists of 64 wt% sulfur, 15.5 wt% $LiCoO_2$, 15.5 wt% graphene and 5 wt% binder. In the following section, the cathode with 64 wt% sulfur was investigated in detail. Note that the standard deviation of capacity is increased slightly with increasing the sulfur fraction, implying that the cathode consistency could be decreased to a certain extent at high sulfur fraction (Fig. 3b).

Before testing the electrochemical performance, the interaction of $LiCoO_2$ host and intermediate polysulfides was examined by immersing $LiCoO_2$ powders in the stoichiometric Li_2S_4 solution for 48 h. After removing the solvent, the chemical state of Li_2S_4/$LiCoO_2$ composite was characterized by XPS. The spectra of Co, O and Li in Li_2S_4/$LiCoO_2$ are almost identical to those of the pristine $LiCoO_2$, indicating the good chemical stability of $LiCoO_2$ in the presence of polysulfides (Fig. S2a–c). In the core level of sulfur, the typical terminal sulfur (S_T^{-1}) at 161.6 eV and bridging sulfur (S_B^{-1}) at 162.7 eV of Li_2S_4 are observed. The slight high valence sulfur at 166.9 and 168.9 eV are attributed to the oxidation by oxygen during the sample transfer process. In the UV-vis spectra of Li_2S_4/$LiCoO_2$ supernatant, a S_4^{2-} peak can also be observed, further confirming the stable existence of S_4^{2-} without side reactions between S_4^{2-} and $LiCoO_2$ (Fig. S3). Impressively, the polar $LiCoO_2$ shows a relatively strong absorption capability than conventional carbon materials, as demonstrated by the weakened S_4^{2-} peak in the UV-vis spectra. Such absorption is expected to alleviate the polysulfides shuttle and benefit the battery cycle stability.

$LiCoO_2$, a typical cathode material in LIBs, is demonstrated to be a superior carbon-free sulfur host in Li-S battery. Fig. 4a shows the CV curves of S/$LiCoO_2$ electrode at 0.1 mV s^{-1}. The two cathodic peaks at 2.30 and 2.04 V are assigned to the reduction of sulfur to polysulfides (Li_2S_x, $4 \leq x \leq 8$) and further to the sulfides (Li_2S_2/Li_2S), respectively. Correspondingly, two anodic peaks at 2.34 and 2.39 V are associated with the oxidation of sulfides to polysulfides and further to sulfur, respectively. The discharge-charge curves of S/$LiCoO_2$ show two typical potential plateaus that indicate the stepwise conversion of sulfur, coinciding well with the CV curves. When the E/S ratio is controlled at 10 μL mg^{-1}, the S/$LiCoO_2$ cathodes with different sulfur loadings of 2.1, 3.6 and 4.8 mg cm^{-2} could deliver desirable gravimetric capacities of 873, 793 and 829 mA h $g^{-1}_{cathode}$ at current densities of 0.17, 0.25, 0.25 mA cm^{-2}, respectively (Fig. 4b), which correspond to areal capacities of 2.9, 4.5 and 6.2 mA h $cm^{-2}_{cathode}$, respectively (Fig. 4c). Moreover, the S/$LiCoO_2$ cathode exhibits a decent cycling stability, with 553 mA h $g^{-1}_{cathode}$ remaining and a high coulombic efficiency over 98% within 100 cycles (Fig. 4d). The long-term stable cycling at 0.1 C rate is also demonstrated by S/$LiCoO_2$ cathodes (2.3 mg cm^{-2} sulfur loading) in Fig. S4. Specifically, with the sulfur loading of 4.8 mg cm^{-2}, the S/$LiCoO_2$ cathode at the current density of 0.5 mA cm^{-2} delivers a high areal capacity of 4.3 mA h $cm^{-2}_{cathode}$ which outperforms the conventional LIBs (~4 mA h cm^{-2}), and keeps an outstanding cycling and a

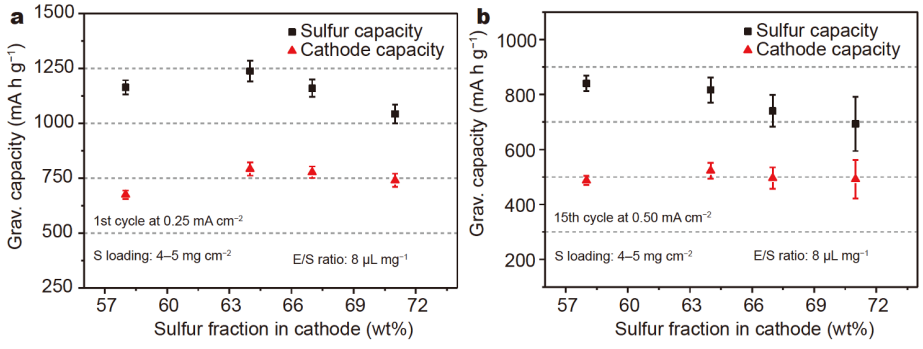

Figure 3 The gravimetric capacities in the 1st (a) and (b) 15th cycles based on sulfur and cathode mass with different sulfur fractions in cathode.

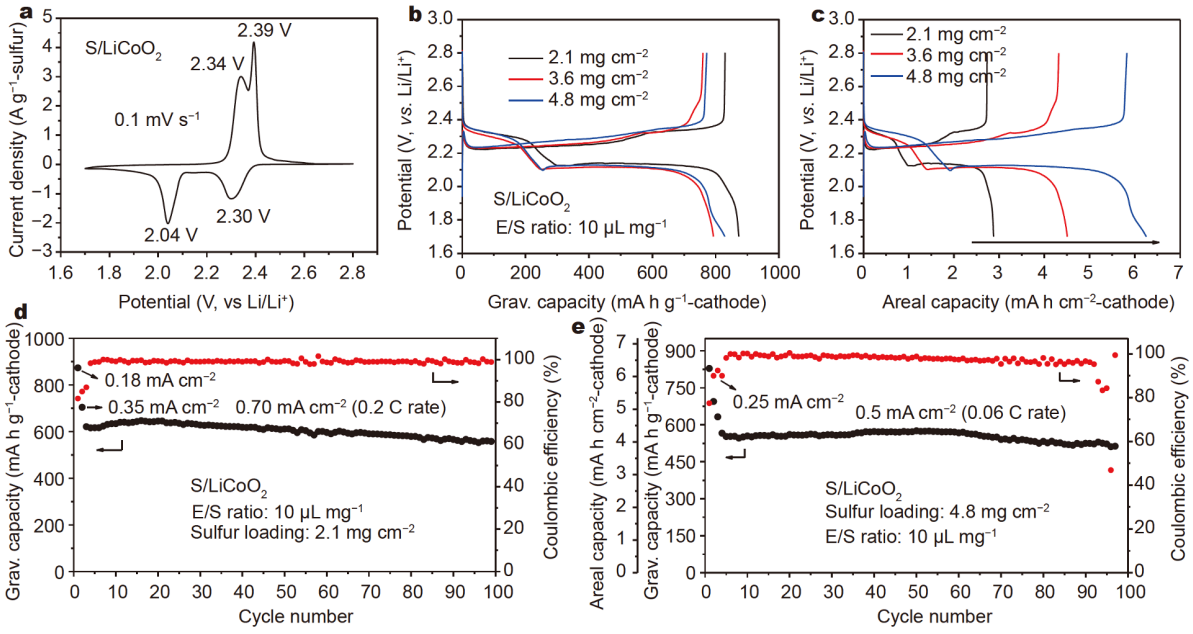

Figure 4 Electrochemical performance of S/$LiCoO_2$ cathode at an E/S ratio of 10 μL mg^{-1}. (a) CV curves at 0.1 mV s^{-1}. Galvanostatic discharge-charge curves based on (b) gravimetric capacity and (c) areal capacity. The current densities are 0.17, 0.25, 0.25 mA cm^{-2} for sulfur loadings of 2.1, 3.6 and 4.8 mg cm^{-2}, respectively. (d) Cycling performance at 0.7 mA cm^{-2} at the sulfur loading of 2.1 mg cm^{-2}. (e) Cycling performance at the current density of 0.5 mA cm^{-2} with the sulfur loading of 4.8 mg cm^{-2}.

coulombic efficiency of ca. 98% over 97 cycles (Fig. 4e).

Electrolyte quantity is highly correlated with the battery performance because of the dissolution-deposition mechanism of sulfur [63]. Abundant electrolyte is beneficial to the fast redox of cathode, but harmful to the energy density of battery. In contrast, lean electrolyte could increase the energy density of battery, but slow down the redox of cathode, which could be called the "electrolyte paradox". Therefore, the S/$LiCoO_2$ cathode under lean electrolyte is further evaluated in the following section, by taking conventional sulfur/carbon nanotube (S/CNT) cathode as a contrast sample. As shown in the CV curves of S/CNT cathode, there are two typical cathodic peaks and two anodic peaks, corresponding to the stepwise reduction and oxidation of sulfur species in ether-based electrolyte (Fig. S5a). As shown in Fig. 5a, the S/$LiCoO_2$ cathode exhibits two typical potential plateaus that suggest its good redox kinetics, with initial discharge capacities of 834, 818 and 790 mA h $g^{-1}_{cathode}$ under E/S ratios of 7, 6 and 5 μL mg^{-1}, respectively. Moreover, the S/$LiCoO_2$ cathode with a sulfur loading of 4.4 mg cm^{-2} has an outstanding cycling with 539 mA h $g^{-1}_{cathode}$ remaining over 69 cycles, much better than the conventional S/CNT cathode (Fig. 5b). The decent electrochemical performance under lean electrolyte indicates the unique superiority of $LiCoO_2$ as carbon-free sulfur host. Besides, the S/$LiCoO_2$ cathode exhibits a good rate performance at E/S ratio of 7 μL mg^{-1}, with high discharge capacities of 704, 605, 547 and 494 mA h $g^{-1}_{cathode}$ at 0.25, 0.5, 1.0 and 1.5 mA cm^{-2}, respectively (Fig. 5c, d). The two potential plateaus during discharge are well maintained at a high current density of 1.5 mA cm^{-2}, indicating a high electrochemical activity of the S/$LiCoO_2$ cathode with lean electrolyte.

Volumetric capacity of S-cathode

Cathode densification is a key factor for Li-S battery to get rid of the low-density drawback from sulfur and carbon, and to achieve a decent balance between W_V and W_G. It is demonstrated that, by adopting heavy $LiCoO_2$ as sulfur host, one can construct a densified S/$LiCoO_2$ cathode. The SEM images in Fig. 6a–d show the top views and cross-sections of the compact S/$LiCoO_2$ cathode and porous S/CNT cathode. At high sulfur loading of 5.1 mg cm^{-2}, the thickness for the S/$LiCoO_2$ and S/CNT cathodes are 89.1 and 173 μm, respectively, resulting in different electrode densities of 0.85 and 0.44 g cm^{-3}, respectively (inset of Fig. 6a, c). Thus, compared with the S/CNT cathode, the S/$LiCoO_2$ cathode has the advantage in electrode densification. The high density of the S/$LiCoO_2$ electrode originally stems from the higher tap density of $LiCoO_2$ (2.26 g cm^{-3}) in comparison to that of CNT

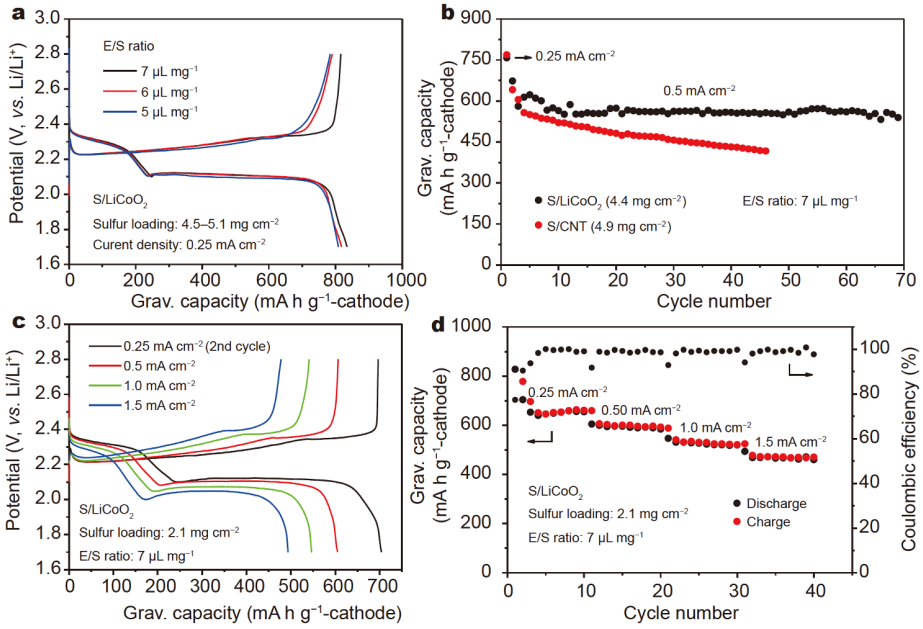

Figure 5 Electrochemical performance of the S/$LiCoO_2$ cathode under lean electrolyte. (a) Galvanostatic discharge-charge curves of cathode with E/S ratios of 7, 6 and 5 μL mg^{-1}. (b) Cycling performance of S/$LiCoO_2$ and S/CNT cathodes with E/S ratio of 7 μL mg^{-1}. (c) Galvanostatic discharge-charge curves of the S/$LiCoO_2$ cathode at different current densities. (d) Rate performance of the S/$LiCoO_2$ cathode with E/S ratio of 7 μL mg^{-1}.

(0.19 g cm^{-3}). More importantly, the compact S/$LiCoO_2$ cathode still exhibits a good electrochemical activity under lean electrolyte (7 μL mg^{-1}), which guarantees the high gravimetric capacity (Fig. S5b). Thus, a balance between densification and electroactivity is obtained through $LiCoO_2$ nanofibers as sulfur host. At the current density of 0.25 mA cm^{-2}, the compact S/$LiCoO_2$ cathode delivers desirable gravimetric/volumetric capacities of 848 mA h g^{-1}/724 mA h cm^{-3}, superior to 724 mA h g^{-1}/324 mA h cm^{-3} of the porous S/CNT cathode (Fig. 6e). By considering the nominal working potential (2.1 V), the cathode could reach high W_V and W_G of 1520 W h L^{-1} and 1781 W h kg^{-1} based on the volume and mass of S/$LiCoO_2$ cathode, respectively, without the current collector. With less electrolyte of 5 μL mg^{-1}, the S/$LiCoO_2$ cathode still achieve decent W_V and W_G (1410 W h L^{-1} and 1659 W h kg^{-1}).

Fig. 6f summarizes the W_V and W_G of both blade cast and freestanding S-cathodes in literatures. All the cathodes have high areal sulfur loadings of above 4 mg cm^{-2}, which is a minimum criterion for practical application. It is suggested that a lower density of the cathode (<0.7 g cm^{-3}) usually leads to high W_G and low W_V, which is the typical case for conventional sulfur/carbon cathodes. While a higher density of the cathode (>1.3 g cm^{-3}) generally gives rise to high W_V and low W_G, which is more common for the compact cathode. For the latter case, the conversion of sulfur in the densified structure is inevitably inhibited because of the difficulty for electrolyte infiltration or limited effective surface area for Li_2S/L_2S deposition [32,45–46]. Therefore, a tradeoff between the cathode density and sulfur utilization should be achieved. Owing to the heavy and catalytic $LiCoO_2$ nanofibers, the S/$LiCoO_2$ cathode can achieve both high density and good electrochemical activity. As a result, a balance between high W_V and W_G is obtained at low E/S ratios, which is superior to all the blade cast cathodes and most of the freestanding cathodes.

Electrochemical redox kinetics

For the S-cathode, fast electrochemical redox kinetics not only ensures a large capacity output by increasing sulfur utilization, but also alleviates the LiPS shuttle and prolongs the cathode life [64]. Therefore, the S/$LiCoO_2$ cathode, with S/CNT as a comparison, was further investigated in terms of the diffusion and charge transfer processes, which are indispensable in sulfur conversion [32,47].

The diffusion process was characterized by CVs at various scan rates from 0.1 to 0.5 mV s^{-1} (Fig. 7a and Fig. S6) [65]. There are two redox couples in the CV curves, which are related to the conversion between sulfur and LiPS (Peak A and D), and the conversion between LiPS and sulfide (Peak B and C). By plotting the peak

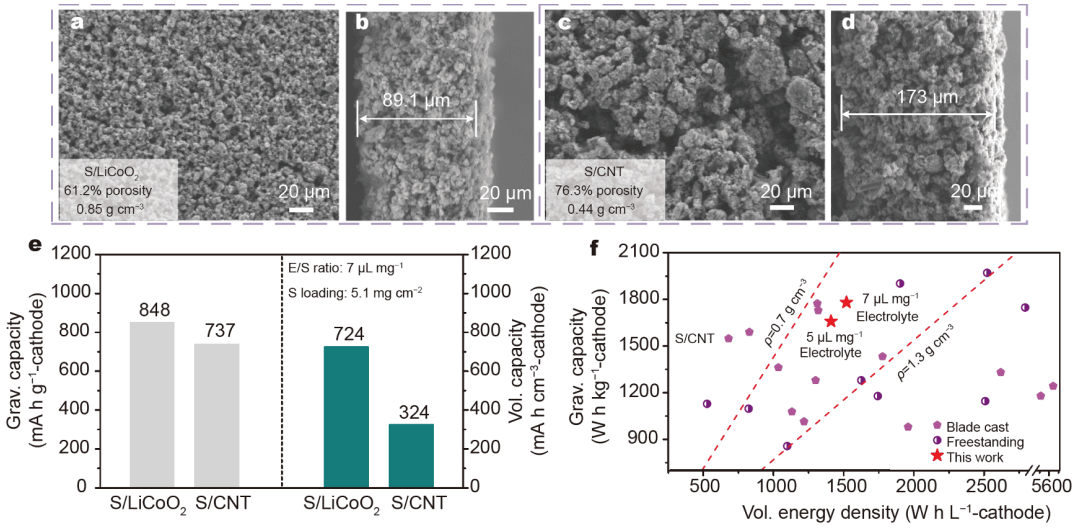

Figure 6 Comparison of gravimetric and volumetric capacity of the S/$LiCoO_2$ and S/CNT cathodes. SEM images of (a, b) S/$LiCoO_2$ and (c, d) S/CNT cathodes. The inset shows the cathode porosity and density. (e) Comparison of gravimetric and volumetric capacities. (f) Summary of high W_V and W_G cathodes in literatures, and the selection criteria is that the sulfur loading should exceed 4 mg cm^{-2}. The energy density was calculated based on the cathode volume and mass without considering the current collector. The detailed data are available in Tables S2, S3 in the Supplementary information.

current against the square root of scan rate, a linear relationship is demonstrated, indicating that the rate-determining step of sulfur reaction is dominated by the diffusion process. Thus, the diffusion behavior could be described by the Randles-Sevcik equation [66]:

$$i_p = (2.69 \times 10^5) n^{3/2} A D_0^{1/2} v^{1/2} C_0^*, \quad (2)$$

where i_p is the peak current (A), n is the charge transfer number, A is the active electrode area (cm^2), D_0 is the lithium ion diffusion coefficient (cm^2 s^{-1}), v is the scan rate (V s^{-1}), and C_0^* is the concentration of LiPS (mol cm^{-3}). The slope of i_p *vs.* $v^{1/2}$ reflects the diffusion rate because n, A and C_0^* are constant in the battery environment. As shown in Fig. 7b, c, the larger slopes for the S/$LiCoO_2$ cathode demonstrate the improved diffusion of LiPS on $LiCoO_2$ host (Fig. 7b, c). Since the Li-S system is mainly controlled by the diffusion process, the improved diffusion of LiPS is indicative of faster reaction of sulfur species.

Charge transfer is a critical process for electrocatalysis of the LiPS redox. The ECSAs of $LiCoO_2$ and CNT electrodes were determined by CV using reversible $K_3[Fe(CN)_6]$ as a probe (Figs S7, S8) [67,68], and the charge transfer was quantitatively evaluated by j_0, which is derived from the LSV using a three-electrode electrochemical cell in 3 mmol L^{-1} Li_2S_4 of 1 mol L^{-1} LiTFSI electrolyte. The *J-V* profiles of $LiCoO_2$ and CNT electrodes are shown in Fig. S9. From the *J-V* curves, the derived j_0 from Tafel plot for $LiCoO_2$ electrode is 1.63×10^{-5} and 2.35×10^{-5} A cm^{-2} for cathodic and anodic polarization, respectively, larger than those for the CNT electrode (1.32×10^{-5} and 0.80×10^{-5} mA cm^{-2}, respectively) (Fig. 7d, e). This suggests that $LiCoO_2$ can act as efficient electrocatalyst for accelerating the charge transfer of intermediate LiPS, indicating a faster redox kinetics (Fig. 7f).

Protection of lithium anode

Generally, the lithium corrosion by diffused LiPS on the anode side is inevitable, and would get more serious when lithium is coupled with thick S-cathode [69]. Therefore, the lithium anode was further investigated with respect to the surface morphology, element distribution and chemical state. After cycling of the cells with different S-cathodes at E/S ratios of 7 μL mg^{-1} and sulfur loadings of 4–5 mg cm^{-2}, the lithium anodes were extracted from the cell for measurement. It is shown that the lithium anode coupled with the S/$LiCoO_2$ cathode has a relatively smooth surface with slight cracks (Fig. 8a), while as a contrast, the lithium anode coupled with the S/CNT cathode shows a rough surface with serious cracks (Fig. 8d). It can be seen from the EDS mappings that the distribution of sulfur and oxygen elements matches well with the surface cracks, suggesting that the lithium cor-

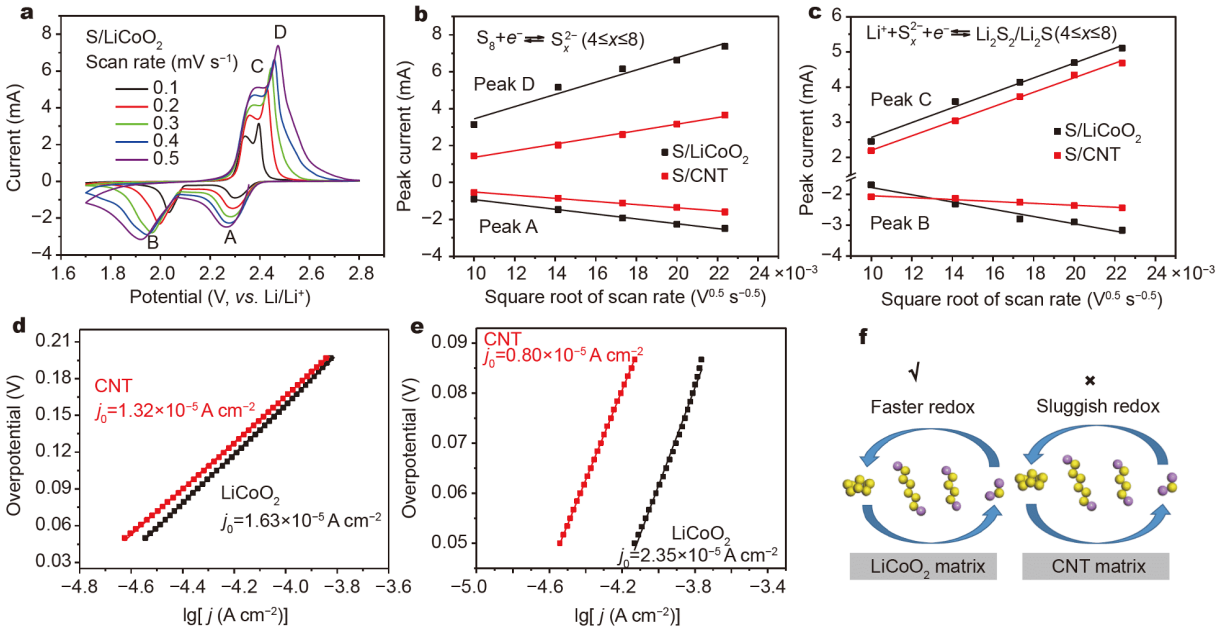

Figure 7 Electrochemical redox kinetics of S/$LiCoO_2$ and S/CNT cathodes. (a) CV curves of the S/$LiCoO_2$ at the scan rates from 0.1 to 0.5 mV s^{-1}. Relationships of square root of scan rate and peak current: (b) Peaks A and D, (c) Peaks B and C. Charge-transfer behavior of lithium polysulfides (Li_2S_4) on $LiCoO_2$ and CNT electrode: Tafel plot in (d) cathodic polarization and (e) anodic polarization. (f) Schematic illustration of fast redox and sluggish redox of sulfur species on $LiCoO_2$ and CNT hosts, respectively.

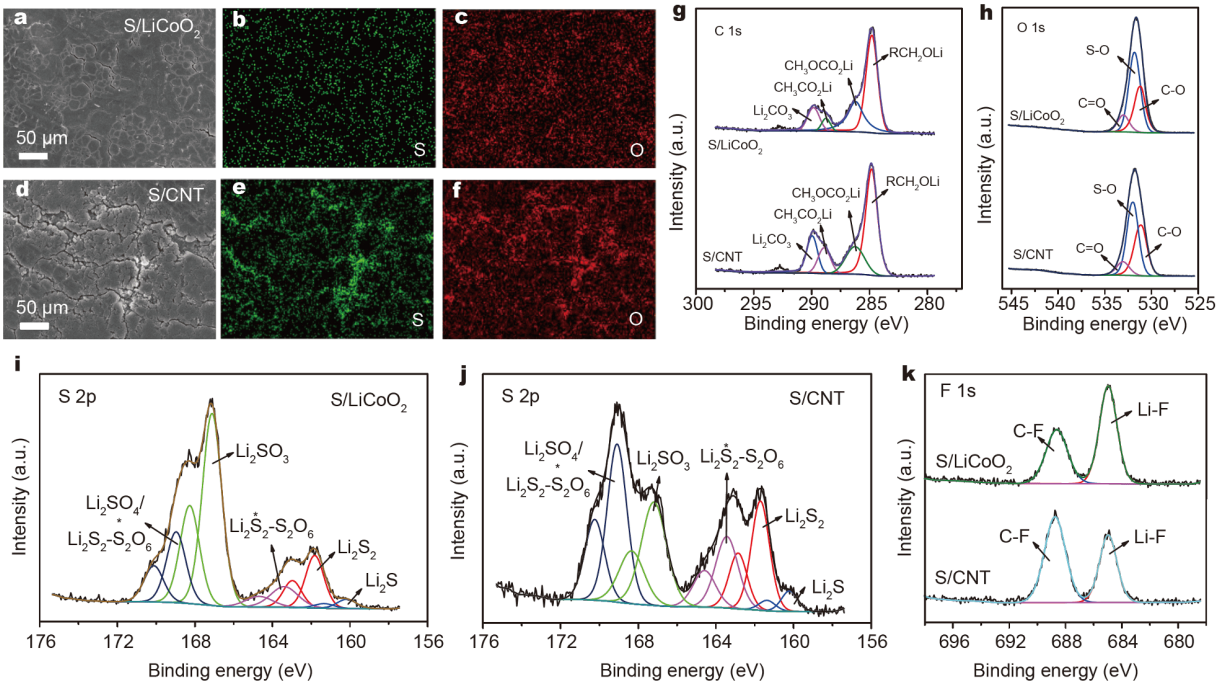

Figure 8 Lithium anode after cycling in the cells with different S-cathodes at E/S ratio of 7 μL mg^{-1} and sulfur loadings of 4–5 mg cm^{-2}. (a) SEM and (b, c) EDS images of lithium surface from the cell with S/$LiCoO_2$ cathode. (d) SEM and (e, f) EDS images of lithium surface from the cell with S/CNT cathode. XPS analysis of the lithium surface: (g) C 1s spectra, (h) O 1s spectra, S 2p spectra of lithium surface from (i) S/$LiCoO_2$ and (j) S/CNT cells and (k) F 1s spectra.

rosion is mainly related to the irreversible deposition of soluble LiPS on the anode side during cycling (Fig. 8b, c, e, f).

In Fig. 8g–k, the chemical compositions of the lithium surfaces are compared based on semi-quantitative XPS analysis. The C 1s spectra show the typical decomposition products of solvents as solid electrolyte interface (SEI) film (Fig. 8g) [70], and the O 1s spectra show the contribution of C–O and S–O bonds with slight C=O bond (Fig. 8h). In S $2p_{3/2}$ core level, two sulfur environments are observed, including the low valence sulfides from the chemical reaction of lithium and LiPS (Li_2S at 160.18 eV and Li_2S_2 at 161.82 eV), and the high valence sulfur species from the LiPS oxidation by $LiNO_3$ (163.39, 167.12 and 168.97 eV) (Fig. 8i, j) [70–72]. For lithium anode coupled with the S/$LiCoO_2$ cathode, the low fraction of sulfides is in coincidence with the smooth surface, indicating the suppressed LiPS shuttling during cycling. Herein, the suppressed shuttling could be originally attributed to the improved electrochemical kinetics of the S/$LiCoO_2$ cathode as revealed in Fig. 7. In F 1s spectra, the peaks at 684.98 and 688.63 eV are attributed to the formation of inorganic Li–F and organic C–F bonds, respectively (Fig. 8k). Since LiF is the key composition of the SEI film [73], the large fraction of LiF implies the more stable SEI film on the lithium surface in the cell with S/$LiCoO_2$ cathode.

CONCLUSIONS

In summary, we construct a high density S-cathode using heavy $LiCoO_2$ nanofibers as host material. The tap density of $LiCoO_2$ is as high as 2.26 g cm^{-3}, and the resultant S-cathode possesses a high density of 0.85 g cm^{-3}, much higher than that of the conventional S/CNT cathode (0.44 g cm^{-3}). Moreover, $LiCoO_2$ nanofibers can serve as an efficient electrocatalyst for enhancing the electrochemical conversion of intermediate LiPS, rendering the S-cathode excellent electrochemical performances. As a result, a balance between the compact structure and good electroactivity is obtained for the S/$LiCoO_2$ cathode, which exhibits both higher gravimetric capacity and volumetric capacity along with good cycling stability, superior to the conventional S/CNT cathode. In addition, the efficient S/$LiCoO_2$ could help to protect lithium anode from irreversibly reacting with polysulfides by alleviating the shuttle effect. Therefore, the present research provides an alternative way for electrode densification, which is critical in achieving both high W_V and W_G for Li-S battery. We do believe that this study would attract more attention on efficient catalytic metal oxides as carbon-free host to further promote their application for Li-S battery.

Received 15 September 2020; accepted 28 October 2020; published online 25 January 2021

1 Bruce PG, Freunberger SA, Hardwick LJ, *et al.* Li–O_2 and Li–S batteries with high energy storage. Nat Mater, 2011, 11: 19–29
2 Gao XP, Yang HX. Multi-electron reaction materials for high energy density batteries. Energy Environ Sci, 2010, 3: 174–189
3 Ji X, Nazar LF. Advances in Li–S batteries. J Mater Chem, 2010, 20: 9821–9826
4 Lochala J, Liu D, Wu B, *et al.* Research progress toward the practical applications of lithium–sulfur batteries. ACS Appl Mater Interfaces, 2017, 9: 24407–24421
5 Zhao M, Li BQ, Zhang XQ, *et al.* A perspective toward practical lithium–sulfur batteries. ACS Cent Sci, 2020, 6: 1095–1104
6 Li Z, Guan BY, Zhang J, *et al.* A compact nanoconfined sulfur cathode for high-performance lithium-sulfur batteries. Joule, 2017, 1: 576–587
7 Zheng G, Zhang Q, Cha JJ, *et al.* Amphiphilic surface modification of hollow carbon nanofibers for improved cycle life of lithium sulfur batteries. Nano Lett, 2013, 13: 1265–1270
8 Li X, Banis M, Lushington A, *et al.* A high-energy sulfur cathode in carbonate electrolyte by eliminating polysulfides *via* solid-phase lithium-sulfur transformation. Nat Commun, 2018, 9: 4509
9 Huang M, Yang J, Xi B, *et al.* Enhancing kinetics of Li-S batteries by graphene-like N,S-codoped biochar fabricated in NaCl non-aqueous ionic liquid. Sci China Mater, 2019, 62: 455–464
10 Ji J, Sha Y, Li Z, *et al.* Selective adsorption and electrocatalysis of polysulfides through hexatomic nickel clusters embedded in N-doped graphene toward high-performance Li-S batteries. Research, 2020, 2020: 1–13
11 Song J, Xu T, Gordin ML, *et al.* Nitrogen-doped mesoporous carbon promoted chemical adsorption of sulfur and fabrication of high-areal-capacity sulfur cathode with exceptional cycling stability for lithium-sulfur batteries. Adv Funct Mater, 2014, 24: 1243–1250
12 Huang S, Lim YV, Zhang X, *et al.* Regulating the polysulfide redox conversion by iron phosphide nanocrystals for high-rate and ultrastable lithium-sulfur battery. Nano Energy, 2018, 51: 340–348
13 Ma L, Chen R, Zhu G, *et al.* Cerium oxide nanocrystal embedded bimodal micromesoporous nitrogen-rich carbon nanospheres as effective sulfur host for lithium–sulfur batteries. ACS Nano, 2017, 11: 7274–7283
14 Wu J, Zhang B, Liu S, *et al.* Grafting polysulfides into a functional *N*-halo compound for high-performance lithium–sulfur battery. Sci China Mater, 2020, 63: 2002–2012
15 Zhang L, Liu Y, Zhao Z, *et al.* Enhanced polysulfide regulation *via* porous catalytic V_2O_3/V_8C_7 heterostructures derived from metal–organic frameworks toward high-performance Li–S batteries. ACS Nano, 2020, 14: 8495–8507
16 Tang T, Zhang T, Zhao L, *et al.* Multifunctional V_3S_4-nanowire/graphene composites for high performance Li-S batteries. Sci China Mater, 2020, 63: 1910–1919
17 Kong W, Yan L, Luo Y, *et al.* Ultrathin MnO_2/graphene oxide/carbon nanotube interlayer as efficient polysulfide-trapping shield for high-performance Li-S batteries. Adv Funct Mater, 2017, 27: 1606663
18 Su YS, Manthiram A. Lithium–sulphur batteries with a microporous carbon paper as a bifunctional interlayer. Nat Commun,

2012, 3: 1166
19 Bai S, Liu X, Zhu K, *et al.* Metal–organic framework-based separator for lithium–sulfur batteries. Nat Energy, 2016, 1: 16094
20 Pei F, Lin L, Fu A, *et al.* A two-dimensional porous carbon-modified separator for high-energy-density Li-S batteries. Joule, 2018, 2: 323–336
21 Li L, Pascal TA, Connell JG, *et al.* Molecular understanding of polyelectrolyte binders that actively regulate ion transport in sulfur cathodes. Nat Commun, 2017, 8: 2277
22 Li G, Ling M, Ye Y, *et al.* *Acacia senegal*-inspired bifunctional binder for longevity of lithium-sulfur batteries. Adv Energy Mater, 2015, 5: 1500878
23 Lin D, Liu Y, Cui Y. Reviving the lithium metal anode for high-energy batteries. Nat Nanotech, 2017, 12: 194–206
24 Li L, Basu S, Wang Y, *et al.* Self-heating–induced healing of lithium dendrites. Science, 2018, 359: 1513–1516
25 Kong LL, Wang L, Ni ZC, *et al.* Lithium–magnesium alloy as a stable anode for lithium–sulfur battery. Adv Funct Mater, 2019, 29: 1808756
26 He D, Liao Y, Cheng Z, *et al.* Facile one-step vulcanization of copper foil towards stable Li metal anode. Sci China Mater, 2020, 63: 1663–1671
27 Progress of lihtium-sulfur battery in Dalian Institute of Chemical Physics, Chinese Academy of Sciences. http://www.cas.cn/syky/201801/t20180115_4632252.shtml (accessed September 2020)
28 Sion power's lithium-sulfur batteries power high altitude pseudo-satellite flight. https://sionpower.com/2014/sion-powers-lithium-sulfur-batteries-power-high-altitude-pseudo-satellite-flight/ (accessed September 2020)
29 OXIS Energy is close to achieving 500Wh/kg and is targeting 600Wh/kg with solid state lithium sulfur technology. https://oxisenergy.com/https-oxisenergy-com-wp-content-uploads-2020-01-500-and-600-whkg-pressor-pdf/ (accessed September 2020)
30 Hagen M, Hanselmann D, Ahlbrecht K, *et al.* Lithium-sulfur cells: The gap between the state-of-the-art and the requirements for high energy battery cells. Adv Energy Mater, 2015, 5: 1401986
31 Xue W, Miao L, Qie L, *et al.* Gravimetric and volumetric energy densities of lithium-sulfur batteries. Curr Opin Electrochem, 2017, 6: 92–99
32 Liu YT, Liu S, Li GR, *et al.* High volumetric energy density sulfur cathode with heavy and catalytic metal oxide host for lithium–sulfur battery. Adv Sci, 2020, 7: 1903693
33 McCloskey BD. Attainable gravimetric and volumetric energy density of Li–S and Li ion battery cells with solid separator-protected Li metal anodes. J Phys Chem Lett, 2015, 6: 4581–4588
34 Zhang C, Yang QH. Packing sulfur into carbon framework for high volumetric performance lithium-sulfur batteries. Sci China Mater, 2015, 58: 349–354
35 Cheng XB, Huang JQ, Zhang Q, *et al.* Aligned carbon nanotube/sulfur composite cathodes with high sulfur content for lithium–sulfur batteries. Nano Energy, 2014, 4: 65–72
36 Zhang C, Liu DH, Lv W, *et al.* A high-density graphene–sulfur assembly: A promising cathode for compact Li–S batteries. Nanoscale, 2015, 7: 5592–5597
37 Li H, Yang X, Wang X, *et al.* Dense integration of graphene and sulfur through the soft approach for compact lithium/sulfur battery cathode. Nano Energy, 2015, 12: 468–475
38 Li H, Tao Y, Zhang C, *et al.* Dense graphene monolith for high volumetric energy density Li-S batteries. Adv Energy Mater, 2018, 8: 1703438
39 Pang Q, Liang X, Kwok CY, *et al.* A comprehensive approach toward stable lithium–sulfur batteries with high volumetric energy density. Adv Energy Mater, 2017, 7: 1601630
40 Yu X, Deng J, Lv R, *et al.* A compact 3D interconnected sulfur cathode for high-energy, high-power and long-life lithium-sulfur batteries. Energy Storage Mater, 2018, 20: 14–23
41 Hu C, Kirk C, Cai Q, *et al.* A high-volumetric-capacity cathode based on interconnected close-packed N-doped porous carbon nanospheres for long-life lithium-sulfur batteries. Adv Energy Mater, 2017, 7: 1701082
42 Li M, Zhang Y, Hassan F, *et al.* Compact high volumetric and areal capacity lithium sulfur batteries through rock salt induced nano-architectured sulfur hosts. J Mater Chem A, 2017, 5: 21435–21441
43 Zhai PY, Huang JQ, Zhu L, *et al.* Calendering of free-standing electrode for lithium-sulfur batteries with high volumetric energy density. Carbon, 2017, 111: 493–501
44 Lu D, Li Q, Liu J, *et al.* Enabling high-energy-density cathode for lithium–sulfur batteries. ACS Appl Mater Interfaces, 2018, 10: 23094–23102
45 Kang N, Lin Y, Yang L, *et al.* Cathode porosity is a missing key parameter to optimize lithium-sulfur battery energy density. Nat Commun, 2019, 10: 4597
46 Lv D, Zheng J, Li Q, *et al.* High energy density lithium-sulfur batteries: challenges of thick sulfur cathodes. Adv Energy Mater, 2015, 5: 1402290
47 Liu YT, Han DD, Wang L, *et al.* $NiCo_2O_4$ nanofibers as carbon-free sulfur immobilizer to fabricate sulfur-based composite with high volumetric capacity for lithium–sulfur battery. Adv Energy Mater, 2019, 9: 1803477
48 Wang ZY, Wang L, Liu S, *et al.* Conductive CoOOH as carbon-free sulfur immobilizer to fabricate sulfur-based composite for lithium–sulfur battery. Adv Funct Mater, 2019, 29: 1901051
49 Zhang Z, Wu DH, Zhou Z, *et al.* Sulfur/nickel ferrite composite as cathode with high-volumetric-capacity for lithium-sulfur battery. Sci China Mater, 2018, 62: 74–86
50 Wang L, Song YH, Zhang BH, *et al.* Spherical metal oxides with high tap density as sulfur host to enhance cathode volumetric capacity for lithium–sulfur battery. ACS Appl Mater Interfaces, 2020, 12: 5909–5919
51 Wang ZY, Han DD, Liu S, *et al.* Conductive RuO_2 stacking microspheres as an effective sulfur immobilizer for lithium–sulfur battery. Electrochim Acta, 2020, 337: 135772
52 Xi K, He D, Harris C, *et al.* Enhanced sulfur transformation by multifunctional FeS_2/FeS/S composites for high-volumetric capacity cathodes in lithium–sulfur batteries. Adv Sci, 2019, 6: 1800815
53 Pang Q, Kundu D, Nazar LF. A graphene-like metallic cathode host for long-life and high-loading lithium–sulfur batteries. Mater Horiz, 2016, 3: 130–136
54 Xue W, Shi Z, Suo L, *et al.* Intercalation-conversion hybrid cathodes enabling Li–S full-cell architectures with jointly superior gravimetric and volumetric energy densities. Nat Energy, 2019, 4: 374–382
55 Xiao Z, Yang Z, Li Z, *et al.* Synchronous gains of areal and volumetric capacities in lithium–sulfur batteries promised by flower-like porous $Ti_3C_2T_x$ matrix. ACS Nano, 2019, 13: 3404–3412
56 Tukamoto H, West AR. Electronic conductivity of $LiCoO_2$ and its enhancement by magnesium doping. J Electrochem Soc, 1997, 144: 3164–3168
57 Zheng X, Chen Y, Zheng X, *et al.* Electronic structure engineering of $LiCoO_2$ toward enhanced oxygen electrocatalysis. Adv Energy

Mater, 2019, 9: 1803482
58 Wang J, Li L, Tian H, *et al.* Ultrathin $LiCoO_2$ nanosheets: An efficient water-oxidation catalyst. ACS Appl Mater Interfaces, 2017, 9: 7100–7107
59 Nie H, Xu L, Song D, *et al.* $LiCoO_2$: recycling from spent batteries and regeneration with solid state synthesis. Green Chem, 2015, 17: 1276–1280
60 Wu B, Wang J, Li J, *et al.* Morphology controllable synthesis and electrochemical performance of $LiCoO_2$ for lithium-ion batteries. Electrochim Acta, 2016, 209: 315–322
61 Heubner C, Nickol A, Seeba J, *et al.* Understanding thickness and porosity effects on the electrochemical performance of $LiNi_{0.6}Co_{0.2}Mn_{0.2}O_2$-based cathodes for high energy Li-ion batteries. J Power Sources, 2019, 419: 119–126
62 Biesinger MC, Payne BP, Lau LWM, *et al.* X-ray photoelectron spectroscopic chemical state quantification of mixed nickel metal, oxide and hydroxide systems. Surf Interface Anal, 2009, 41: 324–332
63 Zhao M, Li BQ, Peng HJ, *et al.* Lithium–sulfur batteries under lean electrolyte conditions: Challenges and opportunities. Angew Chem Int Ed, 2019, 59: 12636–12652
64 Peng L, Wei Z, Wan C, *et al.* A fundamental look at electrocatalytic sulfur reduction reaction. Nat Catal, 2020, 3: 762–770
65 Chung SH, Chang CH, Manthiram A. A carbon-cotton cathode with ultrahigh-loading capability for statically and dynamically stable lithium–sulfur batteries. ACS Nano, 2016, 10: 10462–10470
66 Tao X, Wang J, Liu C, *et al.* Balancing surface adsorption and diffusion of lithium-polysulfides on nonconductive oxides for lithium–sulfur battery design. Nat Commun, 2016, 7: 11203
67 Cui HF, Ye JS, Zhang WD, *et al.* Electrocatalytic reduction of oxygen by a platinum nanoparticle/carbon nanotube composite electrode. J Electroanal Chem, 2005, 577: 295–302
68 Cui HF, Ye JS, Zhang WD, *et al.* Selective and sensitive electrochemical detection of glucose in neutral solution using platinum–lead alloy nanoparticle/carbon nanotube nanocomposites. Anal Chim Acta, 2007, 594: 175–183
69 Cheng XB, Huang JQ, Zhang Q. Review—Li metal anode in working lithium-sulfur batteries. J Electrochem Soc, 2017, 165: A6058–A6072
70 Xiong S, Xie K, Diao Y, *et al.* Characterization of the solid electrolyte interphase on lithium anode for preventing the shuttle mechanism in lithium–sulfur batteries. J Power Sources, 2014, 246: 840–845
71 Lindberg BJ, Hamrin K, Johansson G, *et al.* Molecular spectroscopy by means of ESCA II. Sulfur compounds. Correlation of electron binding energy with structure. Phys Scr, 1970, 1: 286–298
72 Abraham KM, Chaudhri SM. The lithium surface film in the Li/SO_2 cell. J Electrochem Soc, 1986, 133: 1307–1311
73 Fan X, Chen L, Borodin O, *et al.* Non-flammable electrolyte enables Li-metal batteries with aggressive cathode chemistries. Nat Nanotech, 2018, 13: 715–722

Acknowledgements This work was supported by the National Key Research and Development Program (2016YFB0100200), the National Natural Science Foundation of China (21935006 and 21421001), and the Fundamental Research Funds for the Central Universities of China.

Author contributions Liu YT, Wang L and Gao XP conceived the idea. Liu YT designed the research, conducted the experiment, analyzed the data, and wrote the manuscript. Liu S and Li GR analyzed the data. Liu YT and Gao XP revised the manuscript. All the authors contributed to the general discussion.

Conflict of interest The authors declare no conflict of interest.

Supplementary information Supporting data are available in the online version of the paper.

Ya-Tao Liu received his PhD in 2019 from the School of Materials Science and Engineering, Nankai University. His research focused on developing new materials for energy storage technology, especially lithium-sulfur battery.

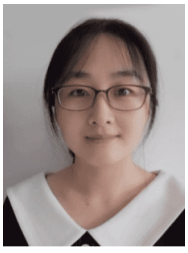

Lu Wang is currently pursuing her doctorate in Prof. Xue-Ping Gao's group at the School of Materials Science and Engineering, Nankai University. She got her Master's degree and Bachelor's degree from Nankai University and Qingdao University, respectively. Her research interests mainly include Li-S battery and perovskite solar cell.

Xue-Ping Gao is a Professor at the Institute of New Energy Material Chemistry, Nankai University. He received his doctorate from the Department of Chemistry, Nankai University in 1995. He worked as a visiting research fellow at Kogakuin University in Japan from 1997 to 1999. Currently, his main research is focused on energy storage materials for power sources, including Li-S battery, Li-ion battery, and solar rechargeable battery.

利用钴酸锂构筑高体积比容量和高质量比容量硫电极

刘亚涛[†], 王璐[†], 刘胜, 李国然, 高学平[*]

摘要 锂-硫电池的质量能量密度较高, 但其体积能量密度却并不理想. 为了提高锂-硫电池的体积能量密度, 需要重点改善复合硫电极的结构和密度. 本研究引入高密度的钴酸锂纳米纤维作为硫的载体材料. 钴酸锂的振实密度高达2.26 g cm^{-3}, 硫/钴酸锂电极的密度和孔隙率分别为0.85 g cm^{-3}和61.2%. 研究发现, 钴酸锂是一种优异的电催化剂, 可以加速活性物质硫的反应速率. 因此, 硫/钴酸锂正极兼具致密的电极结构和良好的电化学活性, 其体积能量密度得到显著提升, 并同时保持较高的质量能量密度. 当硫的面负载量为5.1 mg cm^{-2}时, 整体硫/钴酸锂电极的体积和质量比容量分别为724 mA h cm^{-3} 和 848 mA h g^{-1}. 此外, 钴酸锂可以减缓多硫化锂的穿梭并降低多硫化锂对锂负极的腐蚀, 提高锂负极的稳定性.

